Quantum Hall effect in a two-dimensional semiconductor with large spin-orbit coupling

D. Shcherbakov,[1] Jiawei Yang,[1] Shahriar Memaran,[2] Kenji Watanabe,[3] Takashi Taniguchi,[4] Dmitry Smirnov,[2,5] Luis Balicas,[2,5] and Chun Ning Lau[1,*]

[1]*Department of Physics, The Ohio State University, Columbus, Ohio 43210, USA*
[2]*National High Magnetic Field Laboratory, Tallahassee, Florida 32310, USA*
[3]*Research Center for Functional Materials, National Institute for Materials Science, 1-1 Namiki, Tsukuba, Ibaraki 305-0044, Japan*
[4]*International Center for Materials Nanoarchitectonics, National Institute for Materials Science, 1-1 Namiki, Tsukuba, Ibaraki 305-0044, Japan*
[5]*Department of Physics, Florida State University, Tallahassee, Florida 32306, USA*

(Received 14 September 2021; revised 28 January 2022; accepted 8 July 2022; published 26 July 2022)

We perform magnetotransport studies of atomically thin InSe field-effect transistors with large Rashba spin-orbit coupling (SOC), and extract the Landau level (LL) gaps via thermal activation measurements. Surprisingly, the Landau level gaps at even and odd filling factors are extrapolated to have positive and negative intercepts at $B = 0$, respectively, which result from the spin-split Landau spectrum. We also show that for a material with large spin-orbit coupling, its LL gaps may vary nonlinearly and nonmonotonically as a function of magnetic field. Thus, its effective mass and g-factor cannot be reliably extracted using conventional expressions, but depend rather sensitively on the SOC's strength and tunability.

DOI: 10.1103/PhysRevB.106.045307

I. INTRODUCTION

The burgeoning field of spin-orbitronics [1,2] takes advantage of the spin-orbit coupling (SOC) phenomenon, in which an electron moving in an electric field of an inversion symmetry-broken lattice experiences an effective magnetic field in its rest frame, giving rise to spin-split bands even in the absence of an external magnetic field. A large SOC has been employed to engineer novel spintronic and topological devices, such as quantum spin Hall effect, quantum anomalous Hall effect, and spin-orbit torque [1,3,4]. In two-dimensional (2D) materials, SOC has been demonstrated to give rise to a valley Hall effect [5,6] and Ising superconductivity in transition metal dichalcogenides [7]. A large SOC is also at the heart of engineering topological superconductivity by coupling a strong spin-orbit coupled material to s-wave superconductors [8].

One aspect that distinguishes SOC in 2D materials is its tunability; it can be modified by a gate voltage [9–14], proximity [12–14], and layer number [15], giving rise to ever-more-increasing possibilities for tailoring material properties and device functionalities. In GaAs-based semiconductor heterostructures, two effective masses arising from the spin-split bands have been measured by far-infrared cyclotron [16] and quantum oscillations [17] studies. However, the effect of SOC on the Landau level (LL) gaps in the quantum Hall (QH) regime with well-separated charge gaps, another prototypical 2D phenomenon, has been scarcely studied to date.

Here, using atomically thin InSe layers with unprecedented mobility and large, tunable SOC, we study magnetotransport in the quantum Hall regime. Under a large magnetic field B, well-resolved QH plateaus are observed, with well-quantized Hall resistance R_{xy}. Using thermal activation measurements of longitudinal resistance (R_{xx}), we extract the charge gaps Δ of the first three LLs. Surprisingly, for filling factor $\nu = 4$ and 6, $\Delta(B)$ displays positive intercepts at $B = 0$, while the intercepts are negative for $\nu = 3$ and 5. These peculiar behaviors are accounted for by the large SOC that is tuned by an external electric field. Gaps of the lowest LL are anomalously small, suggesting significantly increased effective mass due to electronic interactions. Finally, we show that LL gaps for devices with large SOC may not scale linearly or monotonically with B; thus, care must be taken when extracting band parameters from QH gaps.

II. DEVICE FABRICATION

Atomically thin InSe is a recent addition to the family of 2D materials, with high mobility [18,19] and a thickness-dependent band gap that ranges from 1 to 3 eV [20–22]. Bulk InSe crystals are grown by the Bridgeman method, and are confirmed by transmission electron microscopy to be γ-phase with rhombohedral stacking [15]. Few-layer InSe flakes are exfoliated from bulk crystals onto polydimethylsiloxane stamps. These flakes are picked up by and sandwiched between hexagonal BN sheets. Few-layer graphene is used to achieve ohmic contacts to the semiconductor. The entire stacks are dropped onto Si/SiO_2 substrates, where the degenerately doped Si serves as the back gate. A schematic of the device is illustrated in Fig. 1(a).

III. MAGNETOTRANSPORT DATA

Figure 1(b) presents the differential longitudinal resistance dR_{xx}/dB of a typical four-layer InSe device as a function of

*Corresponding author: lau.232@osu.edu

 ©2022 American Physical Society

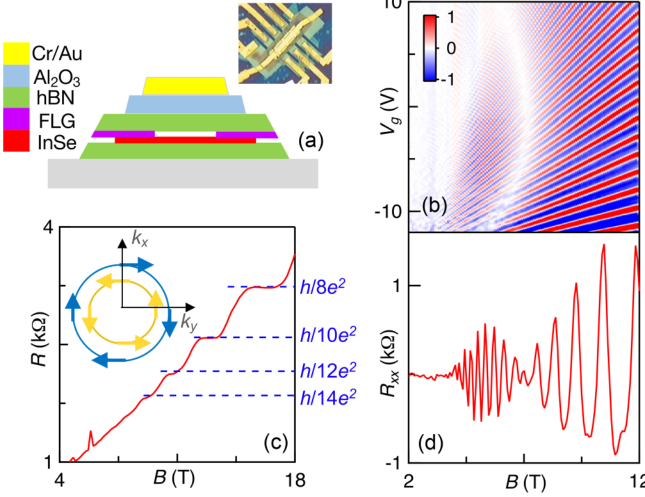

FIG. 1. Schematic and typical transport characteristics of a typical few-layer InSe device. (a) Schematic and optical image of a device. (b) Differentiated longitudinal resistance dR_{xx}/dB versus V_g and B. (c) Hall resistance $R_{xy}(B)$, showing QH plateaus for $8 \leqslant \nu \leqslant 14$. Inset: schematics of spin-split Fermi surfaces from Rashba SOC; the arrows denote spin polarization directions. (d) Line trace dR_{xx}/dB at $V_{bg} = 4.5$ V.

magnetic field B and gate voltage V_g. Prominent Shubnikov–de Haas (SdH) oscillations emerge at $B \sim 3$ T, and quantized Hall resistance plateaus at $B \sim 9$ T, indicating unprecedented mobility [Fig. 1(b) and 1(c)]. An unusual feature of the SdH oscillations is the emergence of beating patterns. As an example, a line trace $\Delta R(B)$ at $V_g = -4.5$ V is shown on Fig. 1(d), where the oscillations' amplitude reaches a node (minimum) at $B \sim 7$ T and increases thereafter. This behavior is part of a beating pattern, arising from the interference of oscillations of two different frequencies, and is indicative of the presence of two distinct Fermi surfaces. As we have demonstrated previously, in InSe, these Fermi surfaces originate from the spin-split bands due to Rashba SOC [15], with dispersion $E = \frac{\hbar k^2}{2m^* m_e} \pm |\alpha k|$ [Fig. 1(c), inset]. Here m^* is the reduced effective mass of charge carriers, m_e is the rest mass of electrons, e is the electron charge, h is the Planck constant, k is the wave vector, and α is the Rashba parameter.

IV. TRANSPORT IN THE QUANTUM HALL REGIME

We now focus on the quantum Hall states in high magnetic fields, where we are able to resolve QH states for filling factors $\nu = 3$ through 6 with well-quantized Hall plateaus [Figs. 2(a) and 2(b)]. Here we present data from a six-layer device D1. To gain insight into the QH states in InSe, we measure $R_{xx}(V_g)$ at different magnetic fields and temperatures T. As temperature increases, valleys in R_{xx} become shallower, but persist up to $T >\sim 60$ K at $B = 25$ T, which are attributed to a combination of the high device quality and the low electronic effective mass [Fig. 2(c)]. Figures 2(d) and 2(e) plots R_{xx} versus $1/T$ in an Arrhenius plot at several different B's for filling factors 4 and 5, respectively. We extract the LL gaps by fitting each resistance valley to $R_{xx} = R_0 + Ae^{-\Delta_\nu/2k_BT}$, where $\Delta\nu$ is the LL gap of the QH state at filling factor ν, R_0 is the residual

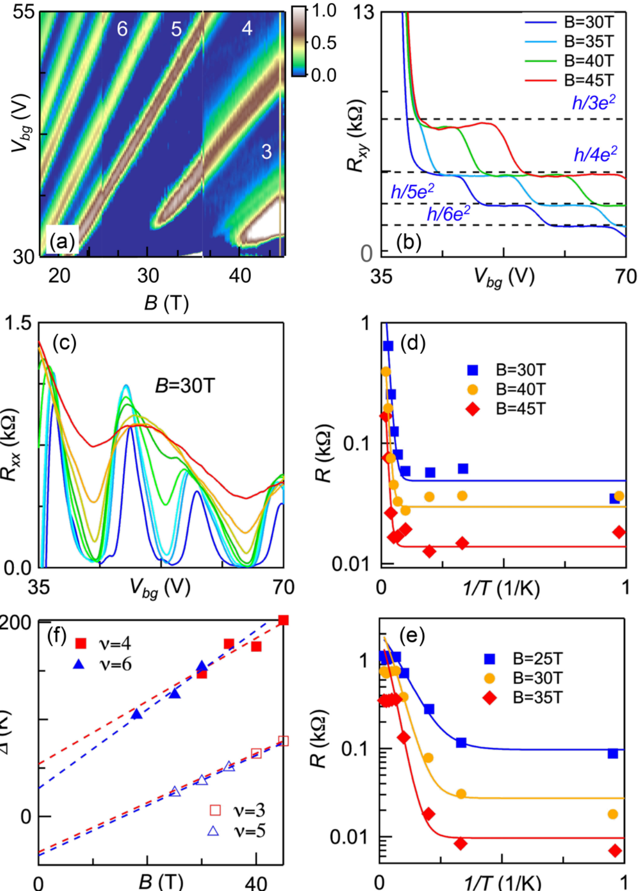

FIG. 2. Magnetotransport data of a six-layer device at high field. (a) $R_{xx}(V_{bg}, B)$ in kiloohms at $T = 0.3$ K. The numbers indicate filling factors. (b) $R_{xy}(V_{bg})$ at different B, showing quantized plateaus. (c) $R_{xx}(V_{bg})$ at $T = 0.5$ K, 3 K, 5 K, 10 K, 15 K, 26 K, 36 K, and 55 K, respectively (bottom to top). (d), (e) Arrhenius plot of R_{xx} versus $1/T$ at different B for $\nu = 4$ and 5, respectively. Traces are offset for clarity. (f) Extracted LL gaps for $\nu = 3$ to 6. The dotted lines are fits to straight lines.

resistance, and k_B is the Boltzmann constant [Figs. 2(d) and 2(f)]. The extracted gap values for $\nu = 3$ through 6 are shown as a function of B in Fig. 2(e). For conventional semiconductors with two-fold spin degeneracy, the LL gaps are

$$\Delta_{\text{odd}} = g\mu_B B - 2\Gamma_\nu$$

and

$$\Delta_{\text{even}} = \hbar\omega_c - g_0\mu_B B - 2\Gamma\nu, \quad (1)$$

where g is the effective Landé factor that can be enhanced from its bare electron value $g_0 = 2$ through exchange interactions, μ_B is the Bohr magneton, $\omega_c = eB/m^*m_0$ is the cyclotron frequency, e is the electron charge, and $\Gamma_\nu > 0$ is the LL broadening. For even filling factors, since the highest filled LL is unpolarized, the Landé g-factor is assumed to adopt the bare value of $g_0 = 2$.

Fitting the data points to Eq. (1), the slopes of $\Delta(B)$ yield an extracted effective mass that varies from 0.25 at $\nu = 6$ to 0.35 at $\nu = 4$ and a g-factor $\sim$4, which are considerably enhanced from their bare values. The variation in m^*

TABLE I. Summary of measured LL gaps and extracted g and m^* values.

Device	ν	Δ_ν (K/T)	Using Eq. (1)		Using Eq. (4)	
			g	m^*	g	m^*
$V_{bg} = 75$ V	1	1.0 ± 0.1	1.5		1.3	
($\alpha = 3.5 \times 10^{-11}$ eV m, $\alpha' = 3.1$ e nm^2)	2	2.5 ± 0.2	2	0.35	1.3	0.40
No top gate	3	2.54	3.8		3.7	
($\alpha = 0.3 \times 10^{-11}$ eV m, $\alpha' = 1.1$ e nm^2)	4	3.24 ± 0.3	2	0.29	3.7	0.22
	5	2.5 ± 0.4	3.7		3.8	
	6	4.1 ± 0.6	2	0.25	3.8	0.20

at different filling factors could, in principle, be attributed to anharmonicity of the bands, though the values found are larger than those found in bulk or in few-layer InSe [18,19]. More surprisingly, the fitted lines for $\Delta_{\nu=4}$ and $\Delta_{\nu=6}$ extrapolate to a finite *positive* intercept at $B = 0$, while that for odd filling factors extrapolates to a negative intercept. Conventionally, a positive intercept is usually taken as an indication of a quantum anomalous Hall state whose gap persists to $B = 0$ [23]; however, the absence of topologically nontrivial bands or any discernible features in R_{xy} at $B = 0$ rules out such a scenario.

These anomalous behaviors of the LL gaps prompt us to examine the spin-split bands induced by a large Rashba SOC. The LL spectrum is then given by [4,24,25]

$$E_0 = \frac{1}{2}\hbar\omega_c - \frac{g\mu_B}{2}B$$

and

$$E_N^{\pm} = \hbar\omega_c\left[N \pm \frac{1}{2}\sqrt{(1 - gm^*/2)^2 + N\frac{\Delta_R^2}{E_F\hbar\omega_c}}\right],\ N \geqslant 1. \tag{2}$$

Here, N is the LL index, $\Delta_R = 2|\alpha k_F|$ is the Rashba spin splitting, α is the Rashba parameter, k_F is the Fermi momentum, and E_F is the Fermi energy. In the large B limit, Eq. (2) can be expanded to yield

$$E_N^{\pm} = \hbar\omega_c\left(N \pm \frac{1}{2}\right) \mp \frac{g\mu_B}{2} \pm 2N\alpha^2\eta, \qquad N \geqslant 1,$$

where $\eta = \frac{m^* m_0}{\hbar^2}\frac{1}{1 - gm^*/2}$, thus leading to energy gaps at even and odd filling factors:

$$\Delta_{\text{odd}} = g\mu_B B - 2\nu\alpha^2\eta$$

and

$$\Delta_{\text{even}} = \hbar\omega_c - g\mu_B B + 2\nu\alpha^2\eta. \tag{3}$$

Comparing with Eq. (1), the same g-factor is used for all filling factors in Eq. (3), and the SOC introduces an additional term $\pm 2\nu\alpha^2\eta$, which can give rise to finite intercepts at $B = 0$. Another effect, which is often underappreciated, is the variation of α with magnetic field at a constant filling factor. This arises from α's dependence on the inversion-breaking out-of-plane electric field $E_\perp$, $\alpha = \alpha_0 + \alpha' E_\perp$, where α_0 is the intrinsic Rashba parameter of InSe, and α' parametrizes the effectiveness of the electric field at tuning the SOC coupling. α' can be positive or negative, depending on its orientation relative to the built-in inversion asymmetry of the lattice.

Thus, the magnitude of spin splitting depends not only on charge density, but also on $E_\perp$. Consequently, for a back-gated device, at a given filling factor, n scales with B, giving rise to proportionally increasing $E_\perp$ and thus α. Since the exact values of electric field drop across the InSe flake depends on screening that is density and layer dependent, and requires self-consistent Hartree calculation, here we define $E_\perp = \frac{C_{tg}V_{tg} - C_{bg}V_{bg}}{2\varepsilon_0}$, i.e., electric field as experimentally imposed by the top and back gates without considering the effect of screening (here, C_{tg} and C_{bg} are capacitance per unit area between the gates and InSe, and ε_0 is the permittivity of vacuum). In the QH regime, $E_\perp = \frac{\nu e^2}{(2\varepsilon_0 h)}B \cong (2.2\ \nu B)$ mV/nm.

Summarizing, the presence of Rashba SOC therefore introduces significant modification to LL gaps: in the large B limit, and collecting the dependencies on B and $E_\perp$, Eq. (2) can be expanded to yield energy gaps

$$\Delta_{\text{even}} = \left[\frac{\hbar e}{m^* m_e} - g\mu_B + 8.8 \times 10^{-3}\nu^2\alpha_0\alpha'\eta\right]B + \left[2\nu\alpha_0^2\eta - 2\Gamma_\nu\right] \tag{4a}$$

and

$$\Delta_{\text{odd}} = [g\mu_B - 8.8 \times 10^{-3}\nu^2\alpha_0\alpha'\eta]B - \left[2\nu\alpha_0^2\eta + 2\Gamma_\nu\right]. \tag{4b}$$

Equation (4) differs from the more conventional Eq. (1) in two important aspects. First, for small LL broadening, the LL gaps at even and odd filling factors have positive and negative intercepts at $B = 0$, respectively, which is in good agreement with our data. Second, the "hidden" dependence of α on B in single-gated devices gives rise to an additional linear B term, which has been ignored in prior measurements of LL gaps in 2D semiconductors with large SOC.

We fit the experimental data of Δ at $\nu = 3$ and 5 to Eq. (4b), and extract g-factors of 3.7 and 3.8, respectively, which are significantly enhanced from the bare value of 2. Using these g values, as well as $\alpha_0 = 0.3 \times 10^{-11}$ eV m, and $\alpha' = 1.1 \times 10^{-2}$ e nm^2 from previous measurements [15], we then fit the data of Δ at $\nu = 2$ and 4, and obtain $m^* \sim 0.23$ at $\nu = 4$ and $m^* = 0.21$ at $\nu = 6$. The extracted values of m^* and g obtained by using Eqs. (1) and (4) are summarized in Table I.

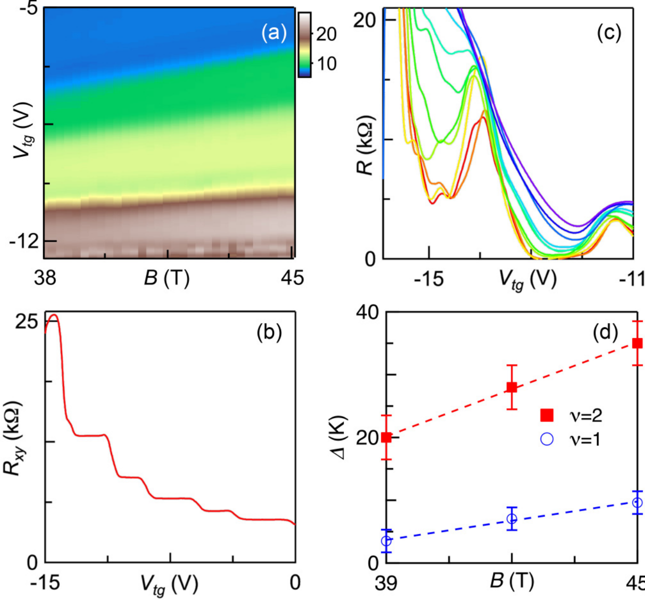

FIG. 3. Thermal activation measurements of LL gaps at high B. (a) $R_{xy}(V_{tg},\ B)$ in kΩ of a dual-gated device at $T = 0.3$ K and $V_{bg} = 75$ V. (b) $R_{xy}(V_{tg})$ at $B = 45$ T and $T = 0.3$ K. (c) $R_{xx}(n)$ at $T = 0.35$ K, 1.5 K, 2.5 K, 3.8 K, 5.2 K, 7.4 K, 9.7 K, 12.1 K, 19 K, and 25 K (bottom to top). (d) Extracted LL gaps for $\nu = 1$ and 2. The dotted lines are fits to straight lines.

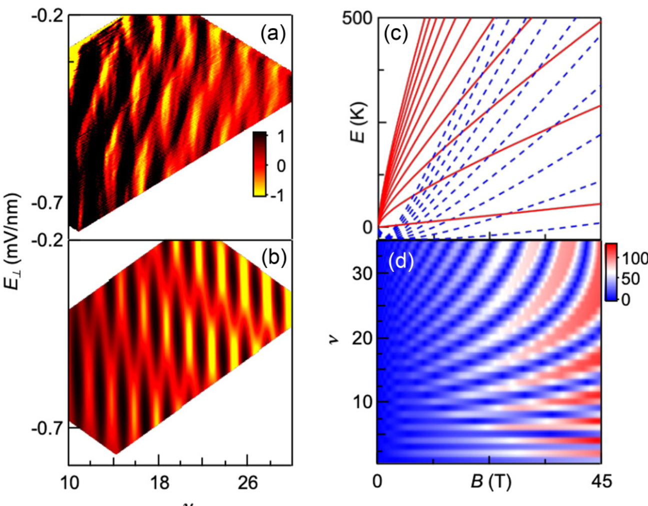

FIG. 4. (a) $dR_{xx}(\nu,\ E_\perp)/dn$ at $B = 10$ T for the dual-gated device. (b) Simulation calculated using $\alpha = 3.5 + 3.0\ E_\perp$, where α is in 10^{-11} eV m and $E_\perp$ in volts per nanometer. (c) Calculated LL spectra using Eq. (2) and $\alpha = 3 \times 10^{-11}$ eV m, $m^* = 0.43$ and $g = 1.3$. (d) Calculated LL gaps Δ in Kelvin vs ν and B using $m^* = 0.43$, $g = 1.3$, $\alpha = (3.5 + 3\ E_\perp) \times 10^{-11}$ eV m and $V_{bg} = 75$ V.

V. QUANTUM HALL GAPS IN THE LOWEST LL AND EFFECT OF SOC

To explore the QH state in the lowest LL, we turn to a dual-gated device. By applying $V_{bg} = 75$ V and tuning the top gate voltages V_{tg}, we are able resolve the QH states $\nu = 1$ and 2. Figure 3(a) displays $R_{xy}(V_{tg},\ B)$ at $V_{bg} = 75$ V. As shown by the line trace $R_{xy}(V_{tg})$ at $B = 45$ T [Fig. 3(b)], well-quantized Hall plateaus with resistance $h/\nu e^2$ are observed. We note that this is the first time that the $\nu = 1$ state is observed experimentally in bulk or atomically thin InSe, again attesting to the quality of the devices. Using thermal activation measurements [Fig. 3(c)], the LL gaps are estimated to be $\Delta_{\nu=2}/B \sim 2.5$ K/T and $\Delta_{\nu=1}/B \sim 1.0$ K/T, respectively [Fig. 3(d)]. If we were to use the more conventional expression Eq. (1), this would yield $m^* = 0.35$ and $g = 1.5$. However, we seek to provide a more accurate account of m^* and g of the lowest LL by taking Rashba SOC-modified band structures into account.

To this end, taking advantage of the dual-gated geometry of the device, we extract both the intrinsic Rashba SOC strength and its tunability by mapping R_{xx} as a function of ν and $E_\perp$ at $B = 10$ T [Fig. 4(a)]. At constant ν, maxima in R_{xx} transition into minima as $E_\perp$ varies, and vice versa; such transition indicate crossings of LLs as α is modulated by $E_\perp$. We can satisfactorily account for the modulation by taking $\alpha = (3.5 + 3.0\ E_\perp) \times 10^{-11}$ eV m [15]. This value of α is sufficiently large that the large-B expansion used in Eq. (4) is no longer valid, even at $B = 45$ T. We therefore numerically calculate the LL gaps at $V_{\mathrm{bg}} = 75$ V using Eq. (2) and $\alpha = 3.5 + 3.0\ E_\perp$, and find that the data are best fit by $m^* = 0.43$ and $g = 1.3$ for $\nu = 1$ and 2. This anomalously large m^* likely arises from strong electronic interactions in the lowest LL at large B. The small g-factor is surprising, since it tends to increase with decreasing charge density in GaAs-based 2D electron gas systems [26]. We currently do not have an explanation for this observation, but note that it may be related to the band's inharmonicity, detailed scattering mechanisms, or electronic interactions in the presence of strong magnetic fields (∼40 to 45 T).

At first glance, the values of g and m^* obtained by fitting to Eqs. (1) and (2) are not significantly different (see Table I). This superficial similarity, however, appears to be coincidental. Generally, materials with large SOC may exhibit LLs that appear to be nonlinear or nonmonotonic with B, due to the SOC-induced LL crossings; this effect is particularly relevant (yet oft-ignored) for devices where only a single gate is used to control the charge density, since $E_\perp$ is inevitably modified in conjunction. A full investigation of LLs in these materials requires two gates to control n and $E_\perp$ independently. To illustrate this point, we plot the LL spectra in Fig. 4(c), which are calculated using Eq. (2), $m^* = 0.43$, $g = 1.3$, and a constant $a = 3.5 \times 10^{-11}$ eV m. The LL energies of the minority and majority carriers, represented by the red solid lines and blue dotted lines, respectively, cross at numerous points. At each crossing, the LL gap vanishes; before (after) the crossing, it decreases (increases) with increasing B, thereby giving rise to a nonmonotonic scaling with B. Moreover, since the LL spectra depend on α, the gate-induced modulation of $E_\perp$ (and therefore α) further modifies the LL gaps. This is captured by the map $\Delta\,(\nu,\ B)$ [Fig. 4(d)], in which the complex dependence of the LL gap on ν and B is illustrated as the color contrast. Evidently, for materials with a large SOC, nonlinear and nonmonotonic dependence on B is the rule rather than exception. Therefore, care must be exercised when extracting band parameters from QH gaps in large spin-orbit coupled materials; fitting data to Eq. (1), particularly over a limited

range or using sparse data points in B, will likely lead to erroneous results.

ACKNOWLEDGMENTS

The experiments are supported by National Science Foundation through Grants No. DMR-2219048 (nanofabrication and quantum transport) and No. DMR-2219003 (material synthesis and characterization). K.W. and T.T. acknowledge support from the Elemental Strategy Initiative conducted by the MEXT, Japan (Grant No. JPMXP0112101001), JSPS KAKENHI (Grant No. JP20H00354) and the CREST (JPMJCR15F3) JST. Part of the crystals are grown at PARADIM. A portion of this work was performed at the National High Magnetic Field Laboratory, which is supported by National Science Foundation Cooperative Agreement No. DMR-1644779, and the state of Florida.

[1] A. Manchon, H. C. Koo, J. Nitta, S. Frolov, and R. Duine, New perspectives for Rashba spin–orbit coupling, Nat. Mater. **14**, 871 (2015).

[2] W. Zhang, M. B. Jungfleisch, W. Jiang, J. Sklenar, F. Y. Fradin, J. E. Pearson, J. B. Ketterson, and A. Hoffmann, Spin pumping and inverse spin Hall effects: Insights for future spin-orbitronics (invited), J. Appl. Phys. **117**, 172610 (2015).

[3] W. Witczak-Krempa, G. Chen, Y. B. Kim, and L. Balents, Correlated quantum phenomena in the strong spin-orbit regime, Annu. Rev. Condens. Matter Phys. **5**, 57 (2014).

[4] R. Winkler, *Spin-orbit Coupling Effects in Two-Dimensional Electron and Hole Systems* (Springer-Verlag, Berlin, 2003).

[5] K. F. Mak, K. L. McGill, J. Park, and P. L. McEuen, The valley Hall effect in MoS_2transistors, Science **344**, 1489 (2014).

[6] J. M. Lu, O. Zheliuk, I. Leermakers, N. F. Q. Yuan, U. Zeitler, K. T. Law, and J. T. Ye, Evidence for two-dimensional Ising superconductivity in gated MoS_2, Science **350**, 1353 (2015).

[7] X. Xi, Z. Wang, W. Zhao, J.- H. Park, K. T. Law, H. Berger, L. Forró, J. Shan, and K. F. Mak, Ising pairing in superconducting $NbSe_2$ atomic layers, Nat. Phys. **12**, 139 (2016).

[8] L. Fu and C. L. Kane, Superconducting Proximity Effect and Majorana Fermions at the Surface of a Topological Insulator, Phys. Rev. Lett. **100**, 096407 (2008).

[9] S. Takasuna, J. Shiogai, S. Matsuzaka, M. Kohda, Y. Oyama, and J. Nitta, Weak antilocalization induced by Rashba spin-orbit interaction in layered III-VI compound semiconductor GaSe thin films, Phys. Rev. B **96**, 161303(R) (2017).

[10] J. Zeng, S.- J. Liang, A. Gao, Y. Wang, C. Pan, C. Wu, E. Liu, L. Zhang, T. Cao, X. Liu, Y. Fu, Y. Wang, K. Watanabe, T. Taniguchi, H. Lu, and F. Miao, Gate-tunable weak antilocalization in a few-layer InSe, Phys. Rev. B **98**, 125414 (2018).

[11] K. Premasiri, S. K. Radha, S. Sucharitakul, U. R. Kumar, R. Sankar, F.- C. Chou, Y.- T. Chen, and X. P. A. Gao, Tuning Rashba spin–orbit coupling in gated multilayer InSe, Nano Lett. **18**, 4403 (2018).

[12] Z. Wang, D.- K. Ki, J. Y. Khoo, D. Mauro, H. Berger, L. S. Levitov, and A. F. Morpurgo, Origin and magnitude of 'designer' spin-orbit interaction in graphene on semiconducting transition metal dichalcogenides, Phys. Rev. X **6**, 041020 (2016).

[13] A. Avsar, J. Y. Tan, J. Balakrishnan, G. K. W. Koon, J. Lahiri, A. Carvalho, A. Rodin, T. Taychatanapat, E. OFarrell, G. Eda, A. H. C. Neto, and B. Ozyilmaz, Spin-orbit proximity effect in graphene, Nat. Commun. **5**, 4875 (2014).

[14] D. Wang, S. Che, G. Cao, R. Lyu, K. Watanabe, T. Taniguchi, C. N. Lau, and M. Bockrath, Quantum Hall effect measurement of spin–orbit coupling strengths in ultraclean bilayer graphene/WSe_2 heterostructures, Nano Lett. **19**, 7028 (2019).

[15] D. Shcherbakov, P. Stepanov, S. Memaran, Y. Wang, Y. Xin, J. Yang, K. Wei, R. Baumbach, W. Zheng, K. Watanabe, T. Taniguchi, M. Bockrath, D. Smirnov, T. Siegrist, W. Windl, L. Balicas, and C. N. Lau, Layer- and gate-tunable spin-orbit coupling in a high-mobility few-layer semiconductor, Sci. Adv. **7**, eabe2892 (2021).

[16] H. L. Stormer, Z. Schlesinger, A. Chang, D. C. Tsui, A. C. Gossard, and W. Wiegmann, Energy Structure and Quantized Hall Effect of Two-Dimensional Holes, Phys. Rev. Lett. **51**, 126 (1983).

[17] J. P. Eisenstein, H. L. Störmer, V. Narayanamurti, A. C. Gossard, and W. Wiegmann, Effect of Inversion Symmetry on the Band Structure of Semiconductor Heterostructures, Phys. Rev. Lett. **53**, 2579 (1984).

[18] E. Kress-Rogers, G. F. Hopper, R. J. Nicholas, W. Hayes, J. C. Portal, and A. Chevy, The electric sub-band structure of electron accumulation layers in InSe from Shubnikov-de Haas oscillations and inter-sub-band resonance, J. Phys. C Solid State Phys. **16**, 4285 (1983).

[19] D. A. Bandurin, A. V. Tyurnina, G. L. Yu, A. Mishchenko, V. Zolyomi, S. V. Morozov, R. K. Kumar, R. V. Gorbachev, Z. R. Kudrynskyi, S. Pezzini, Z. D. Kovalyuk, U. Zeitler, K. S. Novoselov, A. Patane, L. Eaves, I. V. Grigorieva, V. I. Fal'ko, A. K. Geim, and Y. Cao, High electron mobility, quantum Hall effect and anomalous optical response in atomically thin InSe, Nat. Nanotechnol. **12**, 223 (2017).

[20] G. W. Mudd, M. R. Molas, X. Chen, V. Zólyomi, K. Nogajewski, Z. R. Kudrynskyi, Z. D. Kovalyuk, G. Yusa, O. Makarovsky, L. Eaves, M. Potemski, V. I. Fal'ko, and A. Patanè, The direct-to-indirect band gap crossover in two-dimensional van der Waals indium selenide crystals, Sci. Rep. **6**, 39619 (2016).

[21] G. W. Mudd, S. A. Svatek, T. Ren, A. Patane, O. Makarovsky, L. Eaves, P. H. Beton, Z. D. Kovalyuk, G. V. Lashkarev, Z. R. Kudrynskyi, and A. I. Dmitriev, Tuning the bandgap of exfoliated InSe nanosheets by quantum confinement, Adv. Mater. **25**, 5714 (2013).

[22] S. Lei, L. Ge, S. Najmaei, A. George, R. Kappera, J. Lou, M. Chhowalla, H. Yamaguchi, G. Gupta, R. Vajtai, A. D. Mohite, and P. M. Ajayan, Evolution of the electronic band structure and efficient photo-detection in atomic layers of InSe, ACS Nano **8**, 1263 (2014).

[23] Y. Lee, D. Tran, K. Myhro, J. Velasco, Jr., N. Gillgren, C. N. Lau, Y. Barlas, J. M. Poumirol, D. Smirnov, and F. Guinea, Competition between spontaneous symmetry breaking and

single particle gaps in trilayer graphene, Nat. Commun. **5**, 5656 (2014).

[24] Y. A. Bychkov and E. I. Rashba, Properties of a 2D electron gas with lifted spectral degeneracy, JETP **39**, 66 (1984).

[25] Y. A. Bychkov and E. I. Rashba, Oscillatory effects and the magnetic susceptibility of carriers in inversion layers, J. Phys. C Solid State Phys. **17**, 6039 (1984).

[26] T. Ando, A. B. Fowler, and F. Stern, Electronic properties of two-dimensional systems, Rev. Mod. Phys. **54**, 437 (1982).